ChemComm

Accepted Manuscript

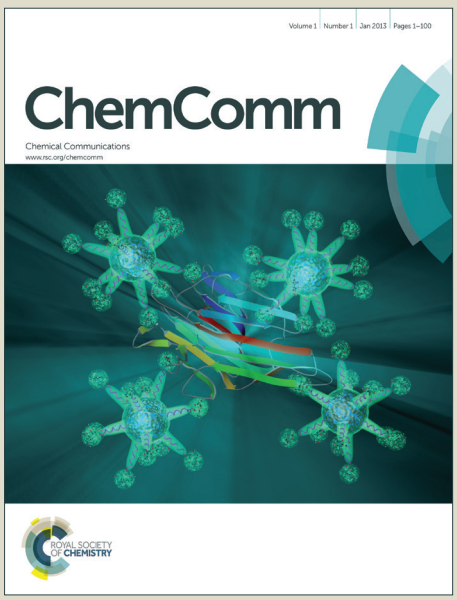

ROYAL SOCIETY OF CHEMISTRY

www.rsc.org/chemcomm

Journal Name

RSCPublishing

COMMUNICATION

Facile synthesis of metal/metal oxide nanoparticles inside nanoporous carbon matrix (M/MO@C) through morphology-preserved transformation of metal-organic framework

Cite this: DOI: 10.1039/xoxxoooooox

Received ooth January 2012,
Accepted ooth January 2012

DOI: 10.1039/xoxxoooooox

www.rsc.org/

Woojeong Bak[a], Hee Soo Kim[a], Hyungphil Chun*[a] and Won Cheol Yoo*[a]

A facile method to transform metal-organic frameworks (MOFs) into metal/metal oxide@carbon (M/MO@C) composites with well-defined shapes is reported. The porosity of carbon and the particle size of M/MO are readily controlled by simple two-step processes that include impregnation of polymer precursors and thermolysis reactions.

Beyond the use of their own features as crystalline porous materials, the utilization of MOFs as a precursor for metal/metal oxide nanoparticles inside carbon framework,[1] or as templates for structural replica has been actively pursued in recent years.[2] The former subject has been of particular interests to the community of materials science because of its implications in practical applications, such as heterogeneous catalysts, CO_2 capture material, anode materials for lithium-ion batteries (LIBs), electrocatalysts for oxygen reduction reaction (ORR) and etc. [3]

Since the Xu group reported the conversion of MOF-5 into porous carbons in 2008,[1] various approaches to design and synthesize structures that contain metal/metal oxide nanoparticles inside porous carbon matrix (M/MO@C) have been attempted. For example, Zn(II)-containing MOFs, such as MOF-5 and ZIF-8 have been used to prepare highly porous carbon materials during which metallic Zn formed *in situ* from the thermolysis of ZnO vaporizes at 900-1000 °C. Such carbon materials have shown promising properties as sorbents for CO_2 or H_2, supercapacitors and electrocatalysts for ORR owing to highly porous nature and heterogeneity of carbon framework, *e.g.* nitrogen doping. Note that these advantages are inherited from the features of MOFs, namely well-defined pore structures and nitrogen-rich organic linkers.[1a, 4]

The next challenge for M/MO@C composites beyond the proof-of-concept stage would be tuning the micro- and meso-porosity of the carbon framework and controlling the size of the M/MO particles while preserving the original morphology of parent MOF crystals. Some of these issues have been tackled by other groups, for example, by using additional carbon source, *e.g.* furfural alcohol[4g] or a two-step calcination process to preserve crystal morphology[3k], and by using aliphatic ligands to control the porosity of M/MO@C composites.[3g] However, a facile synthetic approach that can ideally handle all of the aforementioned issues together has not been reported.

We hereby report a simple method to achieve this goal, and show that composite materials of M/MO@C can readily be synthesized from MOFs. More importantly, the size of the M/MO nanoparticles and the porosities of the host carbon can be readily controlled while maintaining the morphology of the initial MOF crystals. As shown in Scheme 1, our method consists of two simple steps – the formation of phenolic resin inside the nanopores of MOFs through vapor phase polymerization (VPP) followed by thermolysis under an inert atmosphere.

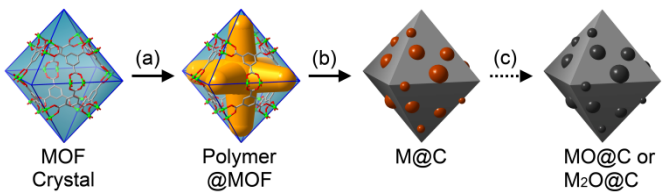

Scheme 1. Shape-persistent transformation of MOF into M/MO@C. MOF undergoes (a) vapor phase polymerization and (b) thermolysis to form M@C composite. (c) A post-thermolytic treatments may turn the metal nanoparticles into oxide species

The porosity of the carbon matrix and the size of M/MO nanoparticles are controlled in the two individual steps, respectively. Details of the morphology-preserved transformation and extensive experimental evidences pertinent to the processes and materials are described below.

In the first step of our work, the activated crystals of the iconic MOF, HKUST-1 ($[Cu_3(btc)_2]$)[5] were exposed to the vapors of phenol and paraformaldehyde under static vacuum at 100 ºC for 24 h. The phenol-formaldehyde (PF) resin had previously been used for nanocasting process in which site-specific polymerization takes place on Al site incorporated in nanoporous silica.[6] In our work, the inclusion of such catalytic sites were unnecessary because the crystalline host contains two open metal sites for every secondary building units which are regularly spaced in a cubic lattice with the

void volume of about 64%. The resulting composite PF@HKUST-1 shows the characteristic X-ray diffraction (XRD) peaks at positions expected from the simulation based on the single-crystal data of HKUST-1 (Figure 1a).

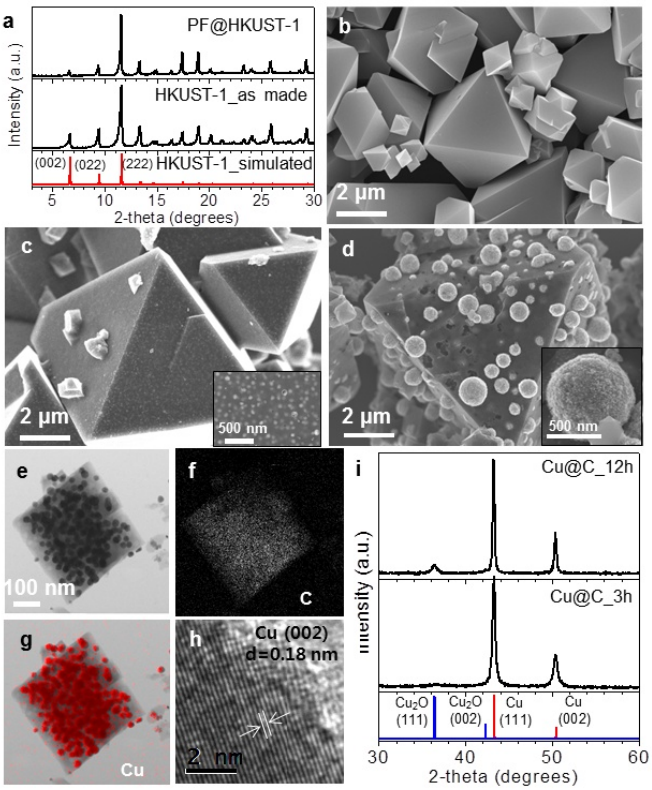

Figure 1. XRD patterns (a) and SEM image (b) of PF@HKUST-1 composite. SEM images of Cu@C obtained by thermolysis for 3 h (c) and 12 h (d). Scanning TEM (e), EDX mapping (f-g) and HRTEM (h) images of Cu@C. (i) XRD patterns of the two samples in (c) and (d).

Scanning electron microscopy (SEM) shows that the octahedral morphology with the highly smooth surface and sharp edges of HKUST-1 has not been affected during the VPP process (Figure 1b). The resin-MOF composite does not adsorb N_2 at 77 K unlike the pristine HKUST-1, while displays a marked increase of organic contents in thermal gravimetric analysis (TGA) (Figure S1). Therefore, the void spaces in HKUST-1 crystals seem to have been completely filled by PF resin without damages to the crystal lattice.

The pale-blue solids of PF@HKUST-1 were then subjected to thermolysis at 800 ºC under pure N_2 atmosphere to obtain a metallic Cu-carbon composite (Cu@C). In this stage, the ramping rates (26, 13 or 4.3 ºC/min) and staying time (1, 3, 6 or 12 h) had been carefully adjusted in order to observe textural differences in the final products. SEM observations on these samples did not reveal a significant change in the appearance of the composite materials regardless of the thermolysis conditions (Figure S2 and S3). When the staying time was 3 h or longer, however, high-contrast spots measuring 40 – 50 nm were found scattered on the surface of the polyhedral carbons in SEM images (Figure 1c). Combined analysis using XRD, high-resolution transmission electron microscopy (HRTEM) and Energy-dispersive X-ray spectroscopy (EDX) on this product revealed that the white spots are metallic Cu spatially dispersed throughout the whole specimens of polyhedral carbons (Figure 1e-i).[7] It has been found out that different ramping rates do not significantly affect the size of the Cu particles which are estimated to be 24 – 29 nm by applying the Scherrer equation to XRD data (Figure S2). On the contrary, prolonged heating at 800 ºC causes the coarsening of particles, and thus results in a consistent increase of the grain size from 26 to 30, 37 and 69 nm on going from 1 to 3, 6 and 12 h, respectively (Figure 1i and S3). The difference between 3 h and 12 h is dramatically shown in the SEM images (Figure 1c-d) in which spherical particles are observed on the surface or partially buried while the sharp edges of the carbon polyhedron are well preserved. We figure that the aggregation of Cu atoms proceeds from inside where the population of metal is relatively high toward outside where the mass transfer experiences less resistance from the carbon framework. For comparison, we carbonized HKUST-1 crystals without the inclusion of PF resin in otherwise the same conditions. As expected, the direct conversion only led to the formation of aggregated Cu particles without any well-defined shape or retention of the crystal morphology (Figure S4).

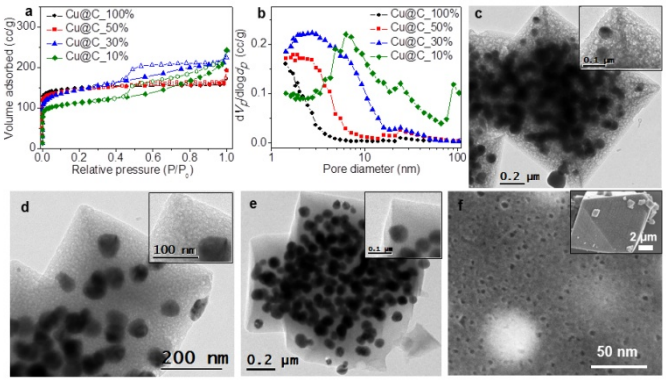

Figure 2. (a) N_2 sorption and (b) BJH pore size distributioins for Cu@C prepared from different PF filling. (c-e) TEM images of Cu@C from 10, 30 and 100% PF filling, respectively. (f) SEM images of Cu@C (10% PF).

The pore size distribution and total pore volume of the carbon matrix in Cu@C can be tuned simply by varying the amount of PF resin included in the first step (Scheme 1). When the amounts of the polymer precursors were reduced to 50, 30 and 10% relative to the one that completely filled the void of HKUST-1 (100%), the pore sizes of the carbon showed a systematic increase (see the supporting information for the detail experimental conditions). This is most directly evidenced by the BJH analysis of N_2 sorption data in which a gradual development of larger mesopores from the initially microporous Cu@C is clearly noticed (Figure 2a-b).

The grain size of Cu particles estimated from XRD data also increases from about 30 nm to 42 nm when the amount of PF resin was reduced to 10%. Under microscopic investigations using SEM and TEM, pores of 10 nm or smaller can be seen on the surface of the carbon polyhedron derived from lower PF contents (10 and 30%) (Figure 2c-d, 2f). This textural feature is completely absent in the TEM images of Cu@C derived from 100% PF filling (Figure 2e). Note that this Cu@C derived from the maximum PF content show a perfect type I N_2 sorption isotherm typical for microporous materials. Consequently, the micropore volume (V_{micro} = 0.24 cm^3/g) accounts

for most of the total pore volume measured at P/P_0 = 0.99 (V_{tot} = 0.26 cm^3/g). Other samples derived from the lower PF contents display varying degree of hysteresis in N_2 sorption which is characteristic of mesopores. Therefore, V_{tot} increases to 0.35 cm^3/g while V_{micro} decreases to 0.12 cm^3/g in the sample prepared with 10% of PF resin. Results of the detailed analysis of the gas sorption data are summarized in Table S1.

The Cu nanoparticles embedded in porous carbon can be readily turned into oxides while the overall morphology is preserved intact. The optimal temperatures for this conversion were determined from the TGA data of Cu@C where the oxidative loss of the carbon matrix starts around 250 ºC in air (Figure S5). Therefore Cu@C was subjected to oxidation at 200 ºC (the ramping rate of 2.9 ºC/min) under the atmosphere of N_2/O_2 mixture (10:1). XRD patterns recorded for the products after 30, 75 and 90 min under this condition show the unmistakable appearance of (111) and (002) diffractions for Cu_2O, along with the gradual disappearance of the characteristic peaks for metallic Cu at 43.2 deg (Figure 3a and S6).

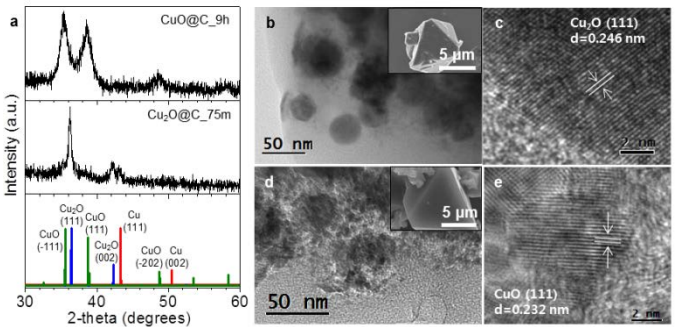

Figure 3. (a) XRD patterns for CuO@C and Cu_2O@C obtained by post-thermolytic treatments for 9 h and 75 min, respectively. (b-c) Low magnification TEM (SEM for inset) and HRTEM images of Cu_2O@C. (d-e) The same set of images for CuO@C.

We note here that diffraction for CuO was not observed in any of these samples. SEM images for this Cu_2O@C show the same morphological and surface features as compared to Cu@C. The (111) fringe of Cu_2O (d = 0.246 nm) observed in HRTEM and the spatial distribution of oxygen, carbon and copper atoms in EDX mapping further confirms the transformation into the oxide species (Figure 3a-c and S6).

When the heating under the mixed gas of N_2 and O_2 was extended beyond 90 min or when fresh Cu@C was heated to 200 ºC (the ramping rate of 2.9 ºC/min) under pure O_2, fully oxidized CuO@C are obtained exclusively. The formation of this Cu(II) oxide phase in well-shaped polyhedral carbon was again independently confirmed by XRD, SEM and HRTEM measurements in which the (111) fringe of CuO (d = 0.233 nm) could be identified (Figure 3a and 3d-e). It is interesting to note that even when the heating at 200 ºC was extended to 9 h from 3 h, the morphology and crystallinity of the CuO@C were well-maintained (Figure S7). Besides, unlike the case of Cu@C, the CuO nanoparticles do not grow in size which is best estimated to be about 7 nm. Instead, some void spaces are observed around the CuO particles in TEM images (Figure S7). More careful investigations using TEM reveal that the void-like spaces are in fact filled by sub-10 nm particles in consistent with the XRD estimation (Figure 3a, 3d-e and S7). We reason that the invariant size of CuO particles is because the microporous framework of carbon allows the passage of oxygen gas but restrict the aggregation of oxide nanoparticles. Controlled transformations of a Mn-based MOF into various manganese oxides having different oxidation states have recently been published;[3i] however, the precise control over the formation of different oxides of a metal by such a simple process as in this work has rarely been known in literature.

In summary, we demonstrated how the morphology of MOF crystals can be transferred to metal or metal oxide–carbon composite materials (M/MO@C) by simple two-step process. The first step is a vapor phase polymerization utilizing the well-defined nanopores of MOFs, and the amount of the polymer filler determines the level of porosity in carbon. The second step is a thermolysis through which the size of embedded metal nanoparticles can be controlled. With HKUST-1, unoxidized Cu@C is obtained which can then be selectively oxidized to either Cu_2O@C or CuO@C. The octahedral morphology of HKUST-1 crystals is preserved throughout these transformations. The method described in this work should be applicable to many other MOFs based on different metals and morphologies. Ultimately, this work may contribute to establishing general synthetic methods for shaped composites consisting of functional nanoparticles interconnected via nanoporous carbon matrix for facile diffusion, which is a highly desired feature in electrode materials and heterogeneous catalysis.

We thank the Basic Science Research Program through the National Research Foundation of Korea (2012R1A1A2004333 for HC and 2014R1A1A2057204 for WCY).

Notes and references

[a] Department of Applied Chemistry, College of Science and Technology, Hanyang University, 55 Hanyangdaehak-ro, Ansan 426-791, Republic of Korea E-mail: hchun@hanyang.ac.kr, E-mail: wcyoo@hanyang.ac.kr

† Electronic Supplementary Information (ESI) available: The complete description of the synthetic procedures and characterization, as well as additional SEM/TEM images and other experimental data. See DOI: 10.1039/c000000x/

1 (a) B. Liu, H. Shioyama, T. Akita, Q. Xu, *J. Am. Chem. Soc.* **2008**, *130*, 5390; (b) W. Cho, Y. H. Lee, J. Lee, M. Oh, *Chem. Commun.* **2009**, 4756; (c) M. Y. Masoomi, A. Morsali, *Coor. Chem. Rev.* **2012**, *256*, 2921; (d) L. Hu, Q. Chen, *Nanoscale* **2014**, *6*, 1236; (e) J.-K. Sun, Q. Xu, *Energy & Environmental Science* **2014**, *7*, 2071. (f) R. Das, P. Pachfule, R. Banerjee, P. Poddar, *Nanoscale* **2012**, *4*, 591.

2 (a) T. Uemura, D. Hiramatsu, Y. Kubota, M. Takata, S. Kitagawa, *Angew. Chem. Int. Ed.* **2007**, *46*, 4987; (b) C. Lu, T. Ben, S. Xu, S. Qiu, *Angew. Chem. Int. Ed.* **2014**, *53*, 6454; (c) A. S. Hall, A. Kondo, K. Maeda, T. E. Mallouk, *J. Am. Chem. Soc.* **2013**, *135*, 16276; (d) G. Distefano, H. Suzuki, M. Tsujimoto, S. Isoda, S. Bracco, A. Comotti, P. Sozzani, T. Uemura, S. Kitagawa, *Nat. Chem.* **2013**, *5*, 335.

3 (a) Y. Lü, W. Zhan, Y. He, Y. Wang, X. Kong, Q. Kuang, Z. Xie, L. Zheng, *ACS Appl. Mater. Interfaces* **2014**, *6*, 4186; (b) W. Cho, S. Park, M. Oh, *Chem. Commun.* **2011**, *47*, 4138; (c) J. M. Zamaro, N. C. Pérez, E. E. Miró, C. Casado, B. Seoane, C. Téllez, J. Coronas, *Chem. Eng. J.* **2012**, *195*, 180; (d) H. B. Wu, S. Wei, L. Zhang, R. Xu, H. H. Hng, X. W. Lou, *Chem. Eur. J.* **2013**, *19*, 10804; (e) W. Chaikittisilp, N. L. Torad, C. Li, M. Imura, N. Suzuki, S. Ishihara, K. Ariga, Y. Yamauchi, *Chem. Eur. J.* **2014**, *20*, 4217; (f) L. Zhang, H. B. Wu, S. Madhavi, H.

H. Hng, X. W. Lou, *J. Am. Chem. Soc.* **2012**, *134*, 17388; (g) T. K. Kim, K. J. Lee, J. Y. Cheon, J. H. Lee, S. H. Joo, H. R. Moon, *J. Am. Chem. Soc.* **2013**, *135*, 8940; (h) R. Wu, X. Qian, F. Yu, H. Liu, K. Zhou, J. Wek, Y. Huang, *J. Mater. Chem. A* **2013**, *1*, 11126; (i) J. H. Lee, Y. J. Sa, T. K. Kim, H. R. Moon, S. H. Joo, *J. Mater. Chem. A* **2014**, *2*, 10435; (j) L. Hu, Y. Huang, F. Zhang, Q. Chen, *Nanoscale* **2013**, *5*, 4186; (k) X. Xu, R. Cao, S. Jeong, J. Cho, *Nano Lett.* **2012**, *12*, 4988.

4 (a) J. Hu, H. Wang, Q. Gao, H. Guo, *Carbon* **2010**, *48*, 3599; (b) W. Chaikittisilp, M. Hu, H. Wang, H.-S. Huang, T. Fujita, K. C.-W. Wu, L.-C. Chen, Y. Yamauchi, K. Ariga, *Chem. Commun.* **2012**, *48*, 7259; (c) S. Lim, K. Suh, Y. Kim, M. Yoon, H. Park, D. N. Dybtsev, K. Kim, *Chem. Commun.* **2012**, *48*, 7447; (d) S. J. Yang, T. Kim, J. H. Im, Y. S. Kim, K. Lee, H. Jung, C. R. Park, *Chem. Mater.* **2012**, *24*, 464; (e) H.-L. Jiang, B. Liu, Y.-Q. Lan, K. Kuratani, T. Akita, H. Shioyama, F. Zong, Q. Xu, *J. Am. Chem. Soc.* **2011**, *133*, 11854; (f) M. Hu, J. Reboul, S. Furukawa, N. L. Torad, Q. Ji, P. Srinivasu, K. Ariga, S. Kitagawa, Y. Yamauchi, *J. Am. Chem. Soc.* **2012**, *134*, 2864; (g) A. Aijaz, N. Fujiwara, Q. Xu, *J. Am. Chem. Soc.* **2014**, *136*, 6790; (h) W. Chen, R. B. Rakhi, M. N. Hedhili, H. N. Alshareef, *J. Mater. Chem. A* **2014**, *2*, 5236.

5 S. S.-Y. Chui, S. M.-F. Lo, J. P. H. Charmant, A. G. Orpen, I. D. Williams, *Science* **1999**, *283*, 1148.

6 (a) W. C. Yoo, A. Stein, *Chem. Mater.* **2011**, *23*, 1761; (b) Z. Wang, F. Li, N. S. Ergang, A. Stein, *Chem. Mater.* **2006**, *18*, 5543; (c) J. Lee, K. Sohn, T. Hyeon, *J. Am. Chem. Soc.* **2001**, *123*, 1546.

7. The small peak of Cu_2O (111) diffraction in Fig. 1i is probably due to the partial oxidation of Cu nanoparticles by residual oxygen originated from the organic filler and ligands. For the presence of residual oxygen in carbon materials prepared by similar methods, see W. C. Yoo, N. Rajabbeigi, E. E. Mallon, M. Tsapatsis, M. A. Snyder, *Microporous Mesoporous Mater.* **2014**, *184*, 72.

